A Cumulus Parameterization Including Mass Fluxes, Convective Vertical Velocities, and Mesoscale Effects: Thermodynamic and Hydrological Aspects in a General Circulation Model

LEO J. DONNER, CHARLES J. SEMAN, AND RICHARD S. HEMLER

NOAA/Geophysical Fluid Dynamics Laboratory, Princeton University, Princeton, New Jersey

SONGMIAO FAN

Program in Atmospheric and Oceanic Sciences, Princeton University, Princeton, New Jersey

(Manuscript received 13 March 2000, in final form 13 March 2001)

ABSTRACT

A cumulus parameterization based on mass fluxes, convective-scale vertical velocities, and mesoscale effects has been incorporated in an atmospheric general circulation model (GCM). Most contemporary cumulus parameterizations are based on convective mass fluxes. This parameterization augments mass fluxes with convective-scale vertical velocities as a means of providing a method for incorporating cumulus microphysics using vertical velocities at physically appropriate (subgrid) scales. Convective-scale microphysics provides a key source of material for mesoscale circulations associated with deep convection, along with mesoscale in situ microphysical processes. The latter depend on simple, parameterized mesoscale dynamics. Consistent treatment of convection, microphysics, and radiation is crucial for modeling global-scale interactions involving clouds and radiation.

Thermodynamic and hydrological aspects of this parameterization in integrations of the Geophysical Fluid Dynamics Laboratory SKYHI GCM are analyzed. Mass fluxes, phase changes, and heat and moisture transport by the mesoscale components of convective systems are found to be large relative to those of convective (deep tower) components, in agreement with field studies. Partitioning between the convective and mesoscale components varies regionally with large-scale flow characteristics and agrees well with observations from the Tropical Rainfall Measuring Mission (TRMM) satellite.

The effects of the mesoscale components of convective systems include stronger Hadley and Walker circulations, warmer upper-tropospheric Tropics, and moister Tropics. The mass fluxes for convective systems including mesoscale components differ appreciably in both magnitude and structure from those for convective systems consisting of cells only. When mesoscale components exist, detrainment is concentrated in the midtroposphere instead of the upper troposphere, and the magnitudes of mass fluxes are smaller. The parameterization including mesoscale components is consistent with satellite observations of the size distribution of convective systems, while the parameterization with convective cells only is not.

The parameterization of convective vertical velocities is an important control on the intensity of the mesoscale stratiform circulations associated with deep convection. The mesoscale components are less intense than in TRMM observations if spatially and temporally invariant convective vertical velocities are used instead of parameterized, variable velocities.

1. Introduction

Many contemporary parameterizations for deep convection used in general circulation models (GCMs) are based on convective mass fluxes (e.g., Arakawa and Schubert 1974; Tiedtke 1989; Gregory and Rowntree 1990; Hack 1994; Zhang and McFarlane 1995). Heat sources and GCM temperature profiles associated with these parameterizations can show reasonable agreement with observations, as, to a somewhat lesser extent, can moisture sinks and humidity profiles (Gregory and Rowntree 1990; Hack 1994; Zhang et al. 1998). This agreement occurs despite the failure of these parameterizations to treat mesoscale processes associated with deep convection. Convective cloud systems with mesoscale components account for large amounts of midlatitude rain and most tropical rain (Houze 1989). The mesoscale components of these cloud systems are closely linked to deep convective towers but are characterized by microphysical, radiative, and dynamic properties that differ from both deep convection and the large-scale flows in which they exist. The success enjoyed by the parameterizations is probably partially a result of compensation for missing mesoscale processes by various large-scale or convective-cell-scale processes.

Corresponding author address: Leo J. Donner, NOAA/Geophysical Fluid Dynamics Laboratory, Princeton University, P.O. Box 308, Princeton, NJ 08542.
E-mail: ljd@gfdl.noaa.gov

Although compensation may occur for heat and moisture sources, adequate treatment of cloud and radiation processes is considerably less likely. Leary and Houze's (1980) analysis shows that the cloud area associated with Global Atmospheric Research Programme (GARP) Atlantic Tropical Experiment (GATE) mesoscale anvils is about 5 times that associated with deep convective cells. Prognostic microphysics are being incorporated in many GCMs (e.g., Smith 1990; Ose 1993; Ricard and Royer 1993; Tiedtke 1993; Le Treut et al. 1994; Boucher et al. 1995; DelGenio et al. 1996; Fowler et al. 1996; Rotstayn 1997; Rasch and Kristjánsson 1998). An important source of condensate for these microphysics parameterizations is deep convection, as demonstrated by satellite measurements showing strong cloud forcing in convectively active regions such as the west Pacific (Harrison et al. 1990). An accurate treatment of the convective sources in these parameterizations requires that the microphysical characteristics of the convective cells be captured, at least in a statistical sense. Since microphysics at the scales of convective cells depends on vertical velocities at cell scales, cumulus parameterizations depending only on mass fluxes lack the key dynamic component driving cell-scale microphysics.

Donner (1993) presents a strategy for parameterizing cell-scale vertical velocities, and thereby microphysics, along with cell-scale mass fluxes. Mesoscale mass fluxes, vertical velocities, and condensate budgets are also treated. Convective cells are represented as an ensemble of elements, each characterized by profiles for mass flux, vertical velocity, microphysical components, temperature, and water-vapor mixing ratio. Cell-scale precipitation and transfers of water vapor and condensate to the mesoscale circulations are computed using this information. The mesoscale circulation is itself dynamically active and generates additional in situ condensate. Donner (1993) applies the parameterization in single columns for the east Atlantic and west Pacific. Alexander and Cotton (1998) use a cloud-system model to design a mesoscale parameterization whose basic framework is similar to Donner (1993).

The purpose of this paper is to apply Donner's (1993) parameterization in a GCM and to evaluate its impact on the thermodynamics and hydrodynamics of the GCM. Radiative aspects of the parameterization, which represent larger differences between it and other parameterizations, will for the most part be left to later studies. Section 2 outlines the details of implementing the parameterization in the Geophysical Fluid Dynamics Laboratory's SKYHI GCM. Section 3 describes experimental integrations designed to exhibit the behavior of the parameterization and isolate the importance of the mesoscale components of convective systems and the parameterization of convective-scale vertical velocities. Section 4 examines heat and moisture sources associated with parameterized convective systems, with special emphasis on the mesoscale components. Section 5 considers the impact of the mesoscale circulations, and section 6 discusses the role of parameterized cumulus-scale vertical velocities. Section 7 compares some of the important subgrid characteristics of the parameterization to observations.

2. Parameterization implementation

The fundamentals of the parameterization are described in Donner (1993). The parameterization is applied there to single columns and is closed using observed precipitation rates. The precipitation rates are used to infer mass fluxes at the bases of members of parameterized cumulus ensembles. Since precipitation rate is a product of the cumulus parameterization in a GCM, these mass fluxes must be parameterized here using a closure. The procedure for obtaining mass fluxes at the bases of ensembles is described in the following paragraphs.

The mass fluxes at cell bases are obtained by requiring that consumption of convective available potential energy (CAPE) by convective systems balances CAPE generation by large-scale flows. CAPE consumption by convective systems is due to *both* cell-scale deep convection *and* associated mesoscale circulations. CAPE generation by the large-scale flow is due to all processes except deep convective systems, including radiation and small-scale surface turbulent fluxes. The vertical velocities and densities at the bases of the convective cells are initial conditions for the steady-state thermodynamic and vertical-momentum equations that describe the cell ensemble, as in Donner (1993). To obtain the cloud-base mass fluxes, only the areas at cloud base are still required.

To obtain the areas at the bases of the convective cells, note that Donner (1993) parameterizes convective-system heat and moisture sources, Q_T and Q_R, respectively:

$$Q_T = c_p^{-1} \sum_{k=1}^{6} L_k \overline{\gamma_k^*} - \pi^{-1} \frac{\partial \overline{\omega' \theta'}}{\partial p}, \quad \text{and} \tag{1}$$

$$Q_R = -\sum_{k=1}^{4} \frac{|L_k|}{L_k} \overline{\gamma_k^*} - \frac{\partial \overline{\omega' q'}}{\partial p}. \tag{2}$$

Here, c_p, refers to specific heat at constant pressure; θ, potential temperature; q, vapor mixing ratio; p, pressure; and $\pi = (p_0/p)^{R_d/c_p}$, where $p_0 = 1000$ hPa and R_d is the gas constant for dry air. The summations are over phase changes γ_1, condensation; γ_2, evaporation; γ_3, deposition (from vapor to ice); γ_4, sublimation; γ_5, freezing; and γ_6, melting. The latent heats of vaporization, sublimation, and fusion are given by L_1, L_3, and L_5. The phase changes are defined to be positive semidefinite, so L_2, L_4, and L_6 are negatively signed for evaporation, sublimation, and melting. Cloud properties are indicated by asterisks; primes indicate departures from large-scale averages, which are in turn denoted by overbars.

Cumulus and mesoscale vertical velocities are used to evaluate (1) and (2), along with the microphysical and thermodynamic properties of the cells and meso-

scale circulations and their areas. The roles of the vertical velocities include driving cell-scale microphysics that partially determine the water budget for the mesoscale circulations. The cell vertical velocities are evaluated using steady-state equations for vertical momentum, in which vertical advection of vertical momentum balances buoyancy, condensate loading, and entrainment. Each ensemble member is characterized by a different entrainment rate. Cumulus-scale pressure gradients are not included. The mesoscale circulations consist of condensate and water vapor detrained from convective cells and water vapor entrained from the large-scale flow into the mesoscale circulations. The ensemble of parameterized cells provides water source terms for the mesoscale circulation directly. The extent to which water vapor in the mesoscale circulation is converted to ice depends on the ascent rates in the mesoscale circulation. The ascent rate is determined by three basic scalings for the mesoscale circulation: its vertical extent, horizontal area, and lifetime. The vertical extent is the distance from the level at which the least-penetrative cell detrains to the upper troposphere. The horizontal area is proportional to the horizontal area of the convective cells (obtained from their vertical velocities and mass fluxes), and the lifetime is set empirically. The mesoscale condensate is partitioned into a component that drives mesoscale downdrafts upon falling from the mesoscale anvil and a component that detrains horizontally into the large-scale flow. The condensate content of the mesoscale circulation is controlled by its water budget; bulk microphysics are employed only for the cells. A full description of the parameterizations for convective cells and mesoscale circulations appears in Donner (1993).

In Donner's (1993) approach, the fractional area $a_1(p_b)$ at the base of an arbitrary member of the ensemble of deep cells can be factored out of the heat and moisture sources:

$$\tilde{Q}_T = \frac{Q_T}{a_1(p_b)}, \quad \text{and} \tag{3}$$

$$\tilde{Q}_R = \frac{Q_R}{a_1(p_b)}. \tag{4}$$

The fractional areas of the members of the ensemble are functions of height, and the fractional areas of other members of the ensemble can be obtained from a_1 using Eq. (23) of Donner (1993). The rate at which CAPE is consumed by convection can be expressed

$$\left[\frac{\partial(\text{CAPE})}{\partial t}\right]_{\text{CON}} = a_1(p_b)I_1, \tag{5}$$

where I_1 is an expression involving vertical integrals of $\tilde{Q}_T$ and $\tilde{Q}_R$. By taking the partial derivative of CAPE with respect to time and relating the convectively generated temperature and mixing-ratio changes in the resulting expression to $\tilde{Q}_T$ and $\tilde{Q}_R$, the detailed form of I_1 is obtained. This expression is presented in appendix B.

The closure (5) is subject to several realizability bounds. There must exist sufficient vapor for it to be satisfied, and the maximum cloud fraction at any height must be no greater than unity. If these conditions cannot be satisfied, the convective system is unable to balance large-scale CAPE generation fully.

There are several requirements imposed before convection can occur. Consistent with (5), $\partial(\text{CAPE})/\partial t$ due to large-scale processes must be positive; CAPE itself must be positive, and I_1 must be negative.

Additional criteria for convection, independent of the closure (5), are also imposed. Two observed characteristics of GATE deep convection suggest that low-level, large-scale ascent is necessary for deep convection in many cases: 1) observed convective inhibition in regions of GATE deep convection was typically around 5 J kg^{-1} (Thompson et al. 1979), and 2) for GATE surface heat fluxes and planetary boundary layer (PBL) depths around 1 km, convective PBL velocities, scaled following Eq. (1.12) of Garratt (1994), are only around 1 m s^{-1}. Thus, boundary layer fluctuations in vertical velocity would be inadequate for near-surface parcels to overcome their convective inhibition. A requirement for large-scale, low-level ascent is imposed:

$$I_2 \leq p_{\text{LFC}} - p_1, \tag{6}$$

where

$$I_2 = \int_{t_0}^{t} \omega(p_1)\, dt. \tag{7}$$

The pressure at the level of free convection (LFC) is denoted as p_{LFC}, while p_1 is the pressure at the first GCM level above the ground. The start time t_0 is reset to zero whenever I_2 becomes zero or $\partial I_2/\partial t > 0$. Requiring that time-integrated, low-level ascent exceed a threshold related to the onset of convection is an element of other cumulus parameterizations (e.g., Kuo 1974). The integral I_2 is obviously a very crude approximation to a Lagrangian parcel trajectory, so an additional requirement that convective inhibition not exceed 10 J kg^{-1} is also imposed. [The threshold value for convective inhibition is based on observations from Thompson et al. (1979).]

Donner's (1993) parameterization is designed for deep convective systems. This is most apparent in its inclusion of a treatment for mesoscale anvils but also is implicit in its use of an entraining plume as its model for cumulus cells. Lin and Arakawa's (1997) trajectory analysis of a cloud-system model indicates continuous entrainment throughout the depth of deep cumulus cells, as expected of entraining plumes. However, observations of nonprecipitating cumulus are not consistent with entraining plumes and suggest much more chaotic mixing for such convection (Raymond and Blythe 1986). Further, the spectrum of entrainment coefficients chosen to partially define the ensemble of cumulus cells in Don-

TABLE 1. SKYHI integrations.

Indentifier	Description
Cell Meso	Convective systems with cells and mesoscale
Cell	Convective systems with cells only
Fixed *w*	Convective systems with cells and mesoscale; no spatial or temporal variation in convective *w*

ner (1993) is drawn from GATE observations of deep convection. Thus, the suitability of Donner's (1993) parameterization for shallow or nonprecipitating convection is probably very limited. A further restriction, requiring that the pressure at the level of zero buoyancy be at least 500 hPa less than at the first model level above the surface, is imposed to limit application of the parameterization to deep convection.

Of course, shallow and nonprecipitating convection play important roles in the atmosphere. The conditions under which they occur are closer to those that saturated adiabatic adjustment (SAA) can treat in GCMs, that is, local convective instability, as opposed to the finite-amplitude instability associated with deep convection. SAA is used in conjunction with Donner's (1993) parameterization to treat shallow and nonprecipitating convection. SAA is applied to layers whose humidity exceeds saturation and whose lapse rate exceeds saturated adiabatic and restores such layers to constant equivalent potential temperature and saturated humidity. Details can be found in the references in Hamilton et al. (1995).

The SKYHI GCM used as a base for the experiments in this paper is described in Donner et al. (1997), except that liquid clouds are treated here following Wetherald (1996). Additional technical aspects of parameterization implementation are described in appendix B.

3. Experimental design

Several experimental integrations are run with SKYHI to demonstrate the general properties of the parameterization and the roles of mesoscale circulations and convective-scale vertical velocities.

The integrations use SKYHI configured as in Donner et al. (1997), except for the changes in parameterization of liquid clouds described in section 2. The integration identified as ''Cell Meso'' employs the Donner (1993) cumulus parameterization, implemented as described in section 2. To illustrate the role of the mesoscale components in deep convective systems, the Cell Meso integration is compared with an integration identified as ''Cell.'' In the Cell integration, the mesoscale component of the Donner (1993) parameterization is deactivated, and the convective systems consist only of convective cells, as in section 2a of Donner (1993). The closure (5) applies in both Cell Meso and Cell Experiments. (Of course, there are no mesoscale contributions to Q_T or Q_R in Cell.)

A distinguishing feature of Donner's (1993) parameterization is its calculation of spatially and temporally

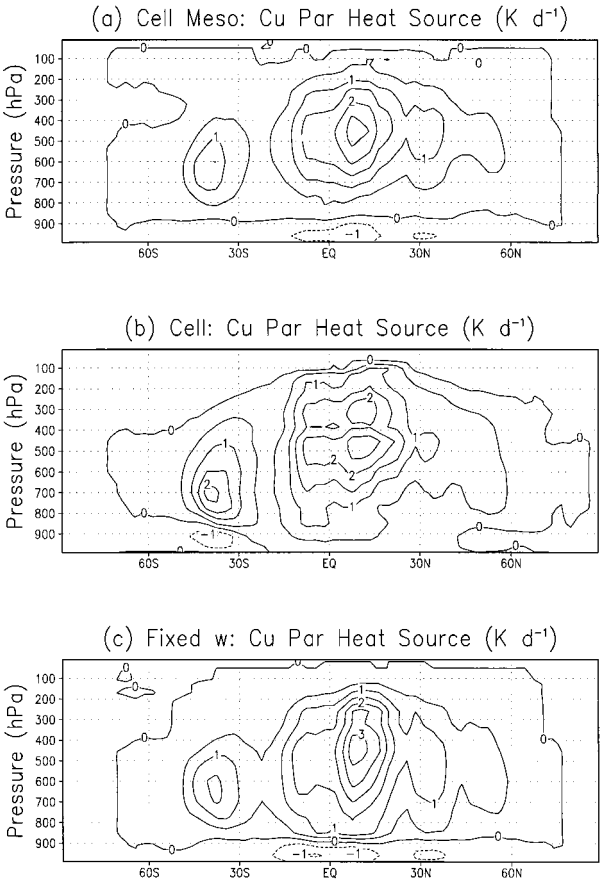

FIG. 1. Heat source Q_T from convective systems for (a) Cell Meso, (b) Cell, and (c) Fixed *w*.

varying convective-scale vertical velocities. The role of these variations in vertical velocity is illustrated using a ''Fixed *w*'' integration. In this integration, the cumulus vertical velocity is assigned a constant value for each member of the cumulus ensemble. The values are different for each ensemble member but do not vary in time or space. One of the obvious advantages of using Donner's (1993) procedure for calculating these vertical velocities using a simplified physical equation for convective vertical velocities is that it avoids the issue of assigning these convective vertical velocities, for which there is no obvious method. For the Fixed *w* integration, a set of oceanic convective vertical velocities is weighted by 70% and a set of land convective vertical velocities is weighted by 30%. The ocean vertical velocities are obtained from LeMone and Zipser (1980), with assignment to ensemble members using a procedure identical to that for assigning entrainment coefficients in Donner (1993). LeMone and Zipser's (1980) oceanic vertical velocities are from GATE, but they are taken here as typical for oceanic convection based on Igau et al.'s (1999) result that the characteristics of oceanic convection were similar in GATE, Tropical Ocean Global Atmosphere Coupled Ocean–Atmosphere Response Ex-

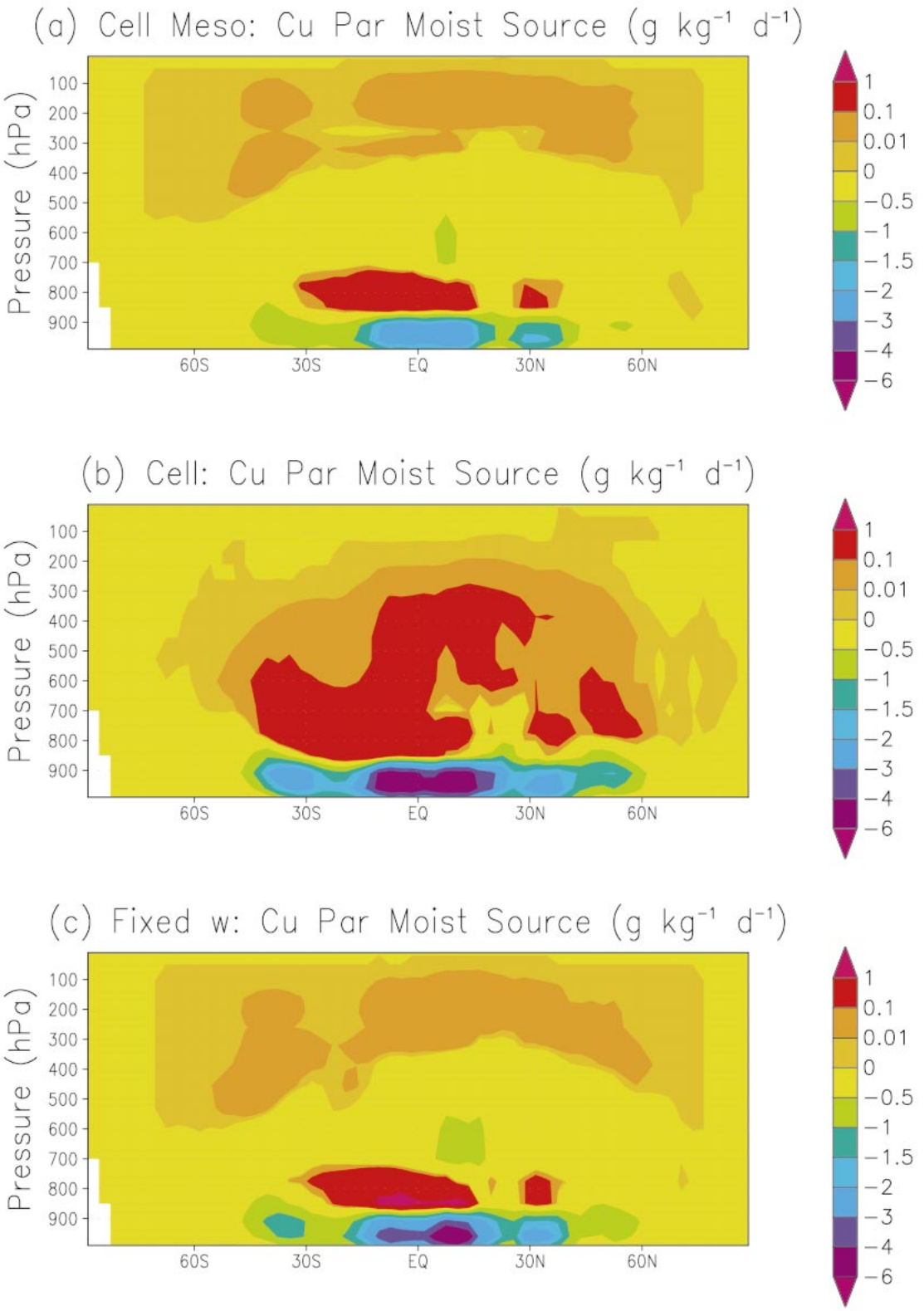

FIG. 2. Moisture source Q_R from convective systems for (a) Cell Meso, (b) Cell, and (c) Fixed w.

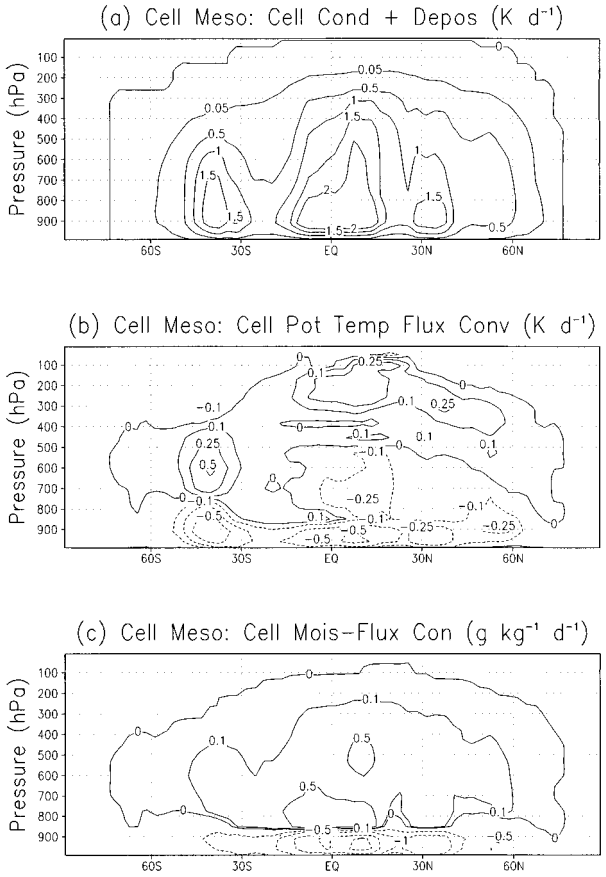

FIG. 3. For Cell Meso, components due to deep convective cells of (a) heating due to condensation and deposition, (b) convergence of potential-temperature flux, $-\pi^{-1}(\partial\overline{\omega'\theta'}/\partial p)$, and (c) convergence of moisture flux, $-\partial\overline{\omega'\theta'}/\partial p$. Contour levels: (a) 0, 0.05, 0.5, 1, 1.5, and 2 K day^{-1}; (b) −0.5, −0.25, −0.1, 0., 0.1, 0.25, 0.5 K day^{-1}; (c) −3, −2, −1, −0.5, 0, 0.1, 0.5 g kg^{-1} day^{-1}.

periment, Equatorial Mesoscale Experiment (EMEX), and the Taiwan Area Mesoscale Experiment (TAMEX). Following Igau et al. (1999, Fig. 4b), continental convective vertical velocities are taken as three times those of oceanic convection but do not exceed 15 m s^{-1}. The ensemble members then have vertical velocities ranging from 4.5 to 11.2 m s^{-1}. Variations in convective vertical velocity are important because convective-scale microphysics is nonlinear with respect to vertical velocity. Note that Fixed *w* already includes a major source of the nonlinear interaction between convective microphysics and vertical velocity by allowing each ensemble member to have its own vertical velocity.

The integrations are summarized in Table 1. All integrations begin on 1 March, extracting these initial conditions from the multiyear SKYHI integration with climatological sea surface temperatures described in Donner et al. (1997). Results shown are averaged for June, July, and August, after a 3-month spinup to allow adjustment to the various combinations of parameterizations employed.

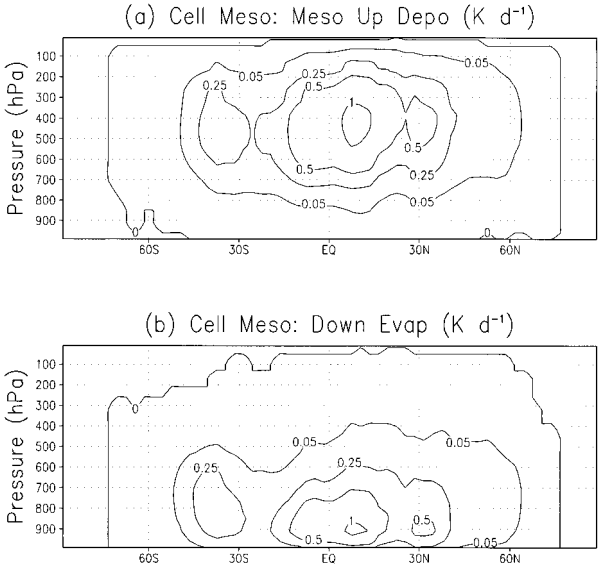

FIG. 4. For Cell Meso: (a) deposition in mesoscale updrafts and (b) evaporation in mesoscale and convective-cell downdrafts.

4. Heat and moisture sources

Heat sources associated with convective systems are illustrated in Fig. 1. (All latitude–height figures in this paper show zonal averages.) The closure (5) is used in

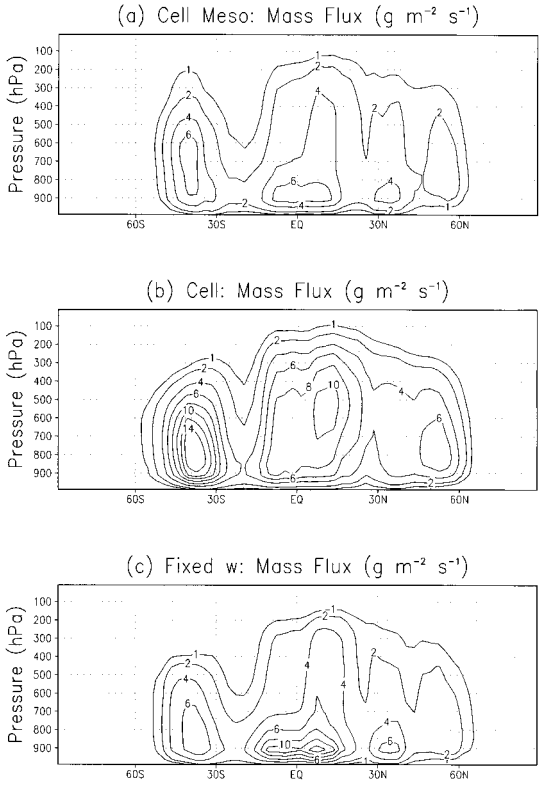

FIG. 5. Convective-system mass fluxes for (a) Cell Meso, (b) Cell, and (c) Fixed *w*.

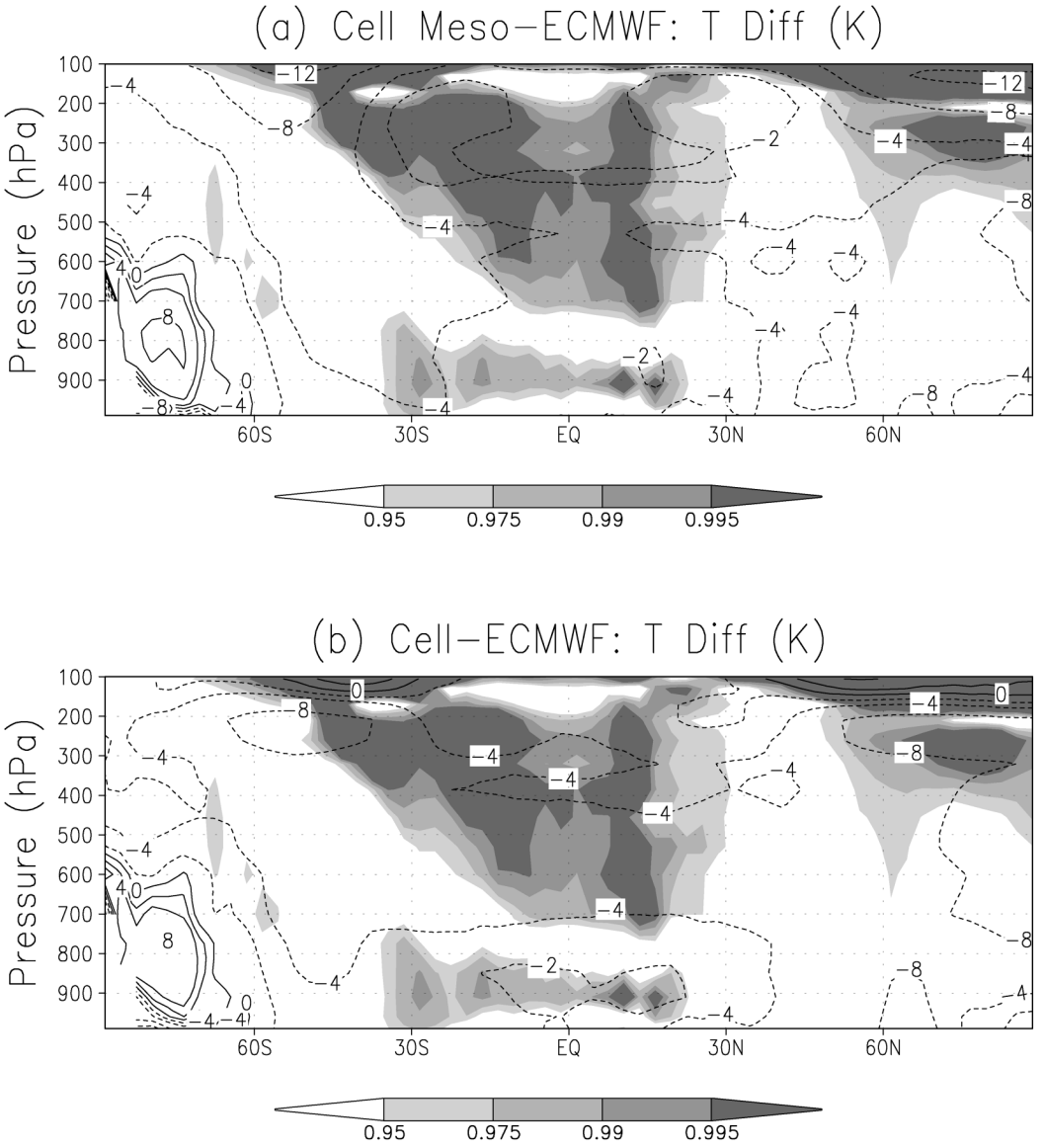

FIG. 6. Temperature differences between (a) Cell Meso and ECMWF analysis and (b) Cell and ECMWF analysis. Mixing-ratio differences between (c) Cell Meso and ECMWF analysis and (d) Cell Meso and ECMWF analysis. Probabilities that differences are significant according to a *t* test are indicated by shading.

all cases, explaining the large amount of similarity between the figures. Clearly, deep cells are able to compensate for the absence of mesoscale circulations in Fig. 1b. As noted in section 1, mass-flux parameterizations generally produce reasonable heat sources without explicit incorporation of mesoscale effects. Figure 1 shows that this would also be true for the Donner (1993) parameterization. Even with identical closures, however, there are some differences in the heat sources. Maximum heating is concentrated at slightly greater heights, and cooling occurs in the tropical PBL in the two integrations that include mesoscale processes.

The corresponding moisture sources are illustrated in Fig. 2. The structures here differ more than for the heat sources. In particular, more drying occurs in the midtroposphere with mesoscale circulations. Moistening persists at pressures lower than 100 hPa with mesoscale circulations, while drying occurs there without them. The latter result stands out in view of the importance of water vapor in the upper troposphere for climate sensitivity (Hall and Manabe 1999). Houze (1989) compiled vertical-velocity profiles for convective systems in tropical oceanic and island cases. The strongest of these systems have nonzero vertical velocities at pressures less than 100 hPa. Donner's (1993) parameterization moistens at pressures this low only when the

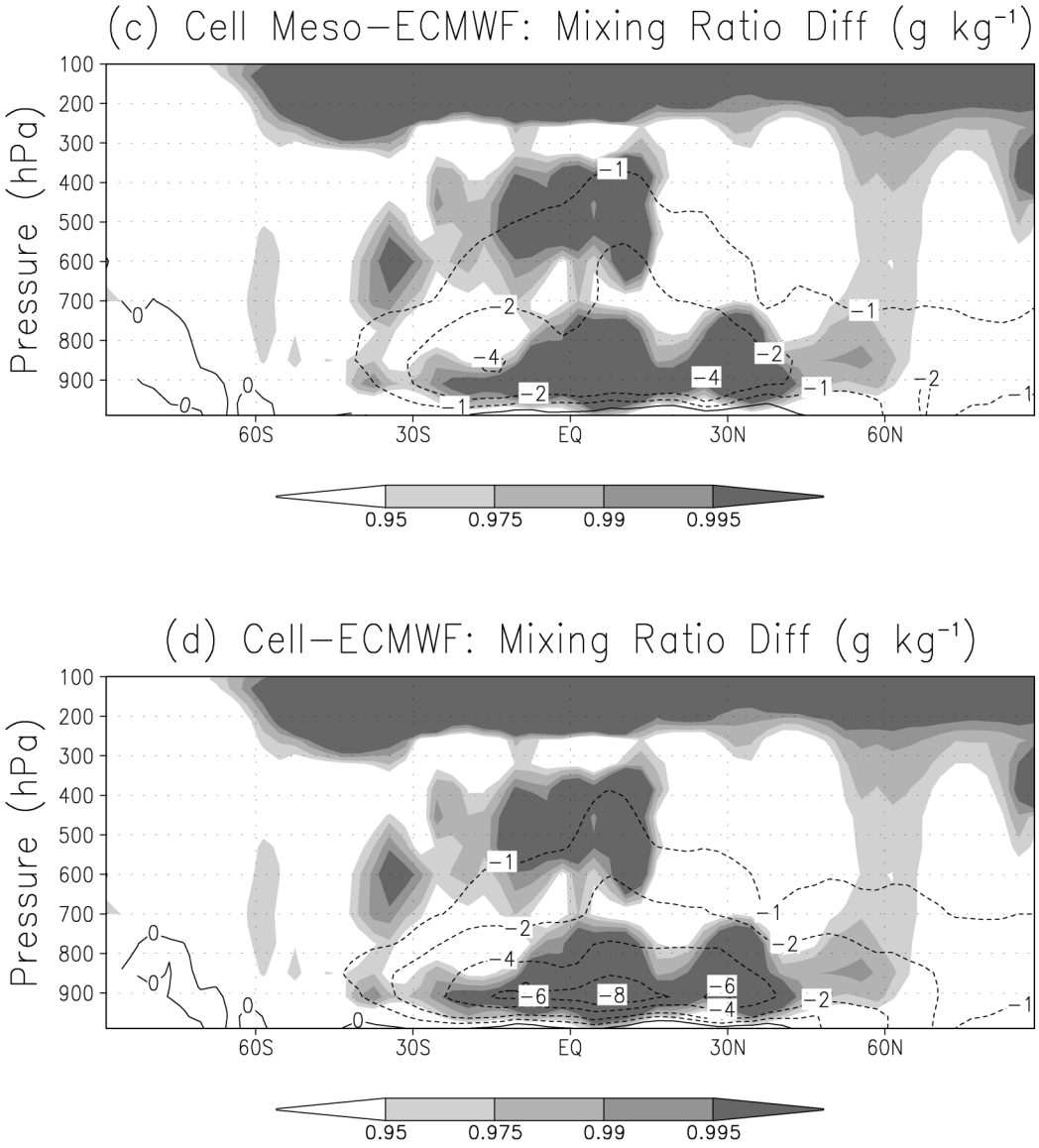

FIG. 6. (*Continued*)

deepest convective cells can penetrate to these pressures. The zonally averaged elevated Cell Meso moisture source is thus consistent with Houze's (1989) profiles. The physical processes composing the heat and moisture sources will be analyzed in detail next.

The cumulus heat and moisture sources consist of two sets of physical mechanisms, phase changes and flux convergence of heat and moisture due to convective systems, which are not resolved by the large-scale flow. Both of these mechanisms occur in convective cells and the associated mesoscale circulations. Figure 3 illustrates the distribution of the dominant processes at the scale of convective cells. Note that the distributions of heating due to phase changes and due to flux convergence of potential temperature are quite different. Both phase changes and flux convergence play important roles as cell-scale sources. Figure 4 shows two of the major mesoscale processes. Note that the magnitudes of the phase changes in both the mesoscale updrafts and downdrafts are appreciable fractions of those in the convective cells themselves. The strong cooling associated with evaporation in downdrafts is evident in the total heat source in Fig. 1, where tropical PBL cooling occurs only when mesoscale processes are parameterized. The cumulus heat sources for Cell and Cell Meso in Figs. 1a,b do not differ by as much as the magnitudes of the mesoscale processes depicted in Fig. 4, however, indicating that, in the Cell integration, convective cells compensate for absent mesoscale processes under the constraint of the same closure.

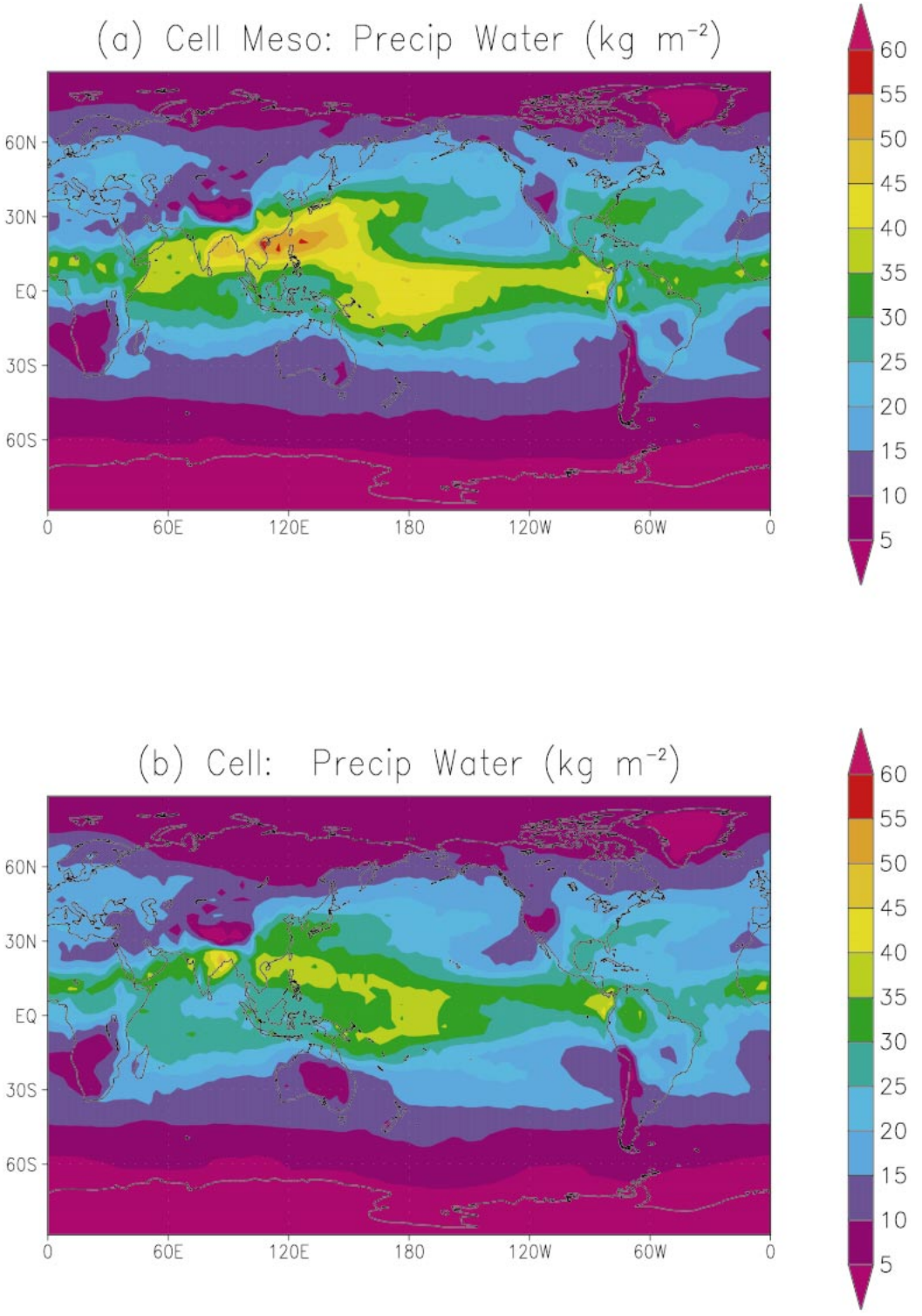

FIG. 7. Precipitable water for (a) Cell Meso, (b) Cell, and (c) NVAP.

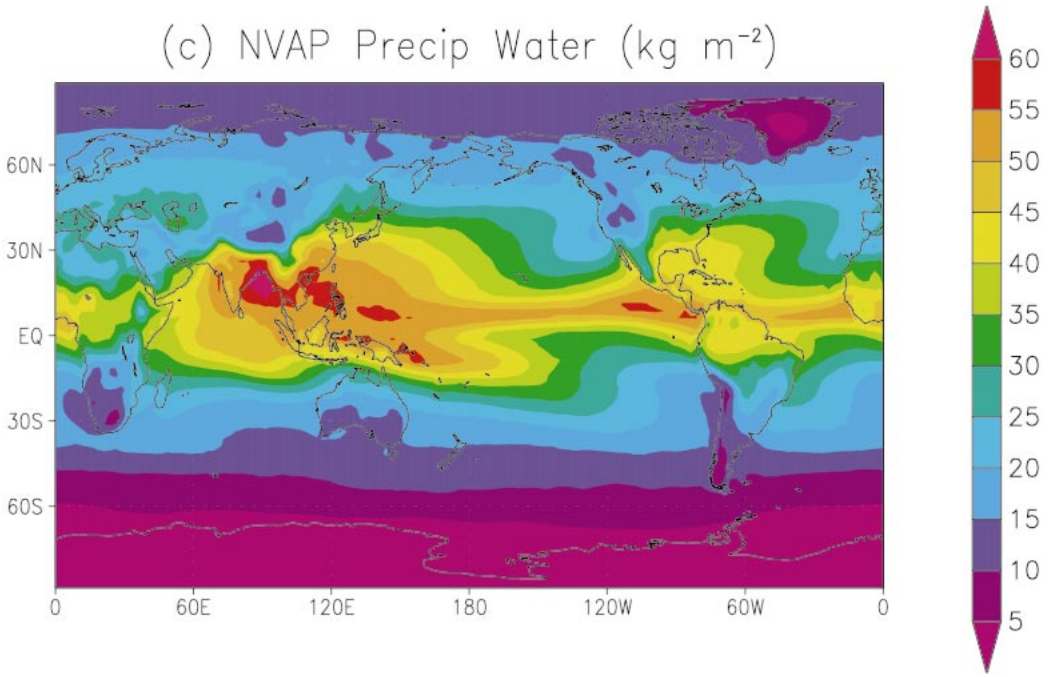

FIG. 7. (*Continued*)

5. Impact of mesoscale circulations

Figures 1 and 2 reveal some differences in the zonally averaged structure of cumulus-parameterization heat and moisture sources when mesoscale processes are not parameterized. These differences are considerably smaller than the magnitudes of heating and cooling associated with the mesoscale processes themselves. This situation does not hold for convective-system mass fluxes (Fig. 5). Total mass fluxes are much weaker when mesoscale processes are active, and their vertical distribution is much different, with largest mass fluxes concentrated in the lower troposphere when mesoscale processes are active and in the mid-to-upper troposphere when only convective cells are active. This result shows that deep convective cells become more active when mesoscale circulations are absent for a given closure, (5) in this case. This increased, compensating activity explains the reasonable success many mass-flux parameterizations have enjoyed in representing heat sources, even though they have neglected mesoscale circulations, which observations have shown to be significant (Houze 1989).

The striking differences in mid- and upper-tropospheric mass fluxes between Cell Meso and Cell (Figs. 5a,b) contrast with the closer cumulus-parameterization heat sources (Figs. 1a,b). This behavior can be explained in terms of the physical processes that compose the cumulus-parameterization heat source. The heat source Q_T in (1) can also be expressed as the sum of a term proportional to the mass flux and a term involving detrainment (Arakawa and Schubert 1974). A convective system with greater detrainment can thus maintain a given heat source with smaller mass fluxes. The mass fluxes for Cell Meso and Cell in Figs. 5a,b illustrate just this behavior.

The significant differences in mass fluxes may have implications for tracer transport by deep convection. Allen et al. (1997) report upper-tropospheric concentrations of carbon monoxide in regions of deep tropical convection exceeding observed concentrations in a chemical transport model employing a mass-flux parameterization lacking mesoscale circulations.

The large-scale temperature and water-vapor fields interact with the cumulus parameterization through the heat and moisture sources depicted in Figs. 1 and 2. Although the differences between Cell Meso and Cell are not nearly as large for these sources as for the mass fluxes, the mesoscale circulations change large-scale fields. Figure 6 illustrates the effects of mesoscale circulations on temperature and mixing ratio. The tropical troposphere is warmer, moister, and generally closer to observations in Cell Meso. The *t*-test significance of the temperature differences between Cell Meso and Cell (using 4-week periods as independent samples) exceeds 0.95 for the tropical troposphere between about 700 hPa and the tropopause and at pressures less than 300 hPa poleward of 60°N.

Evaporation from downdrafts is associated with a much smaller moisture sink in the tropical PBL in Cell Meso, and mixing ratios are as much as 4 g kg^{-1} higher in the lower tropical troposphere. The changes in the lower tropical troposphere are *t*-test significant at 0.995 between the surface and about 800 hPa. The moister

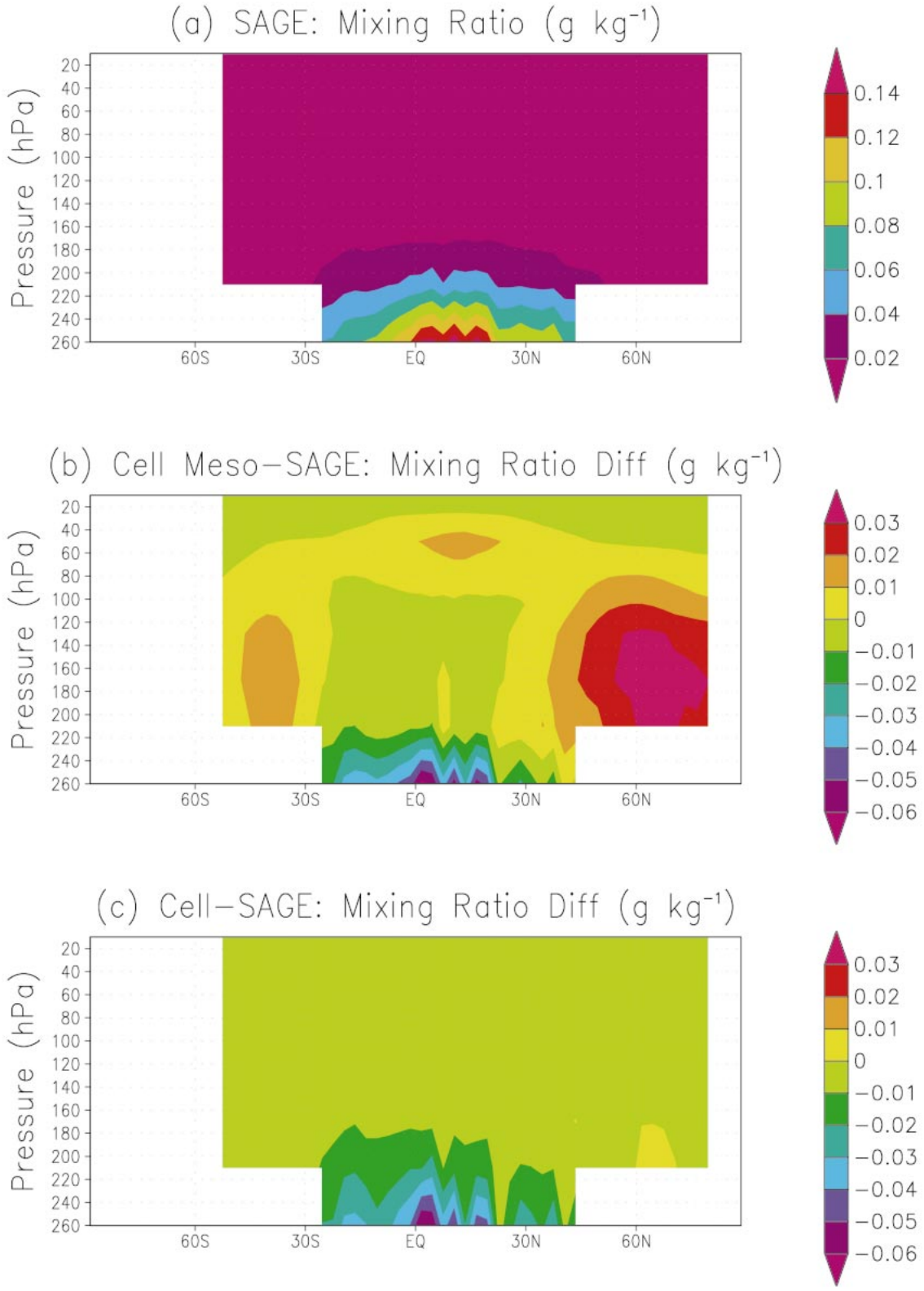

FIG. 8. (a) SAGE mixing ratios. Differences in mixing ratios between (b) Cell Meso and SAGE and (c) Cell and SAGE.

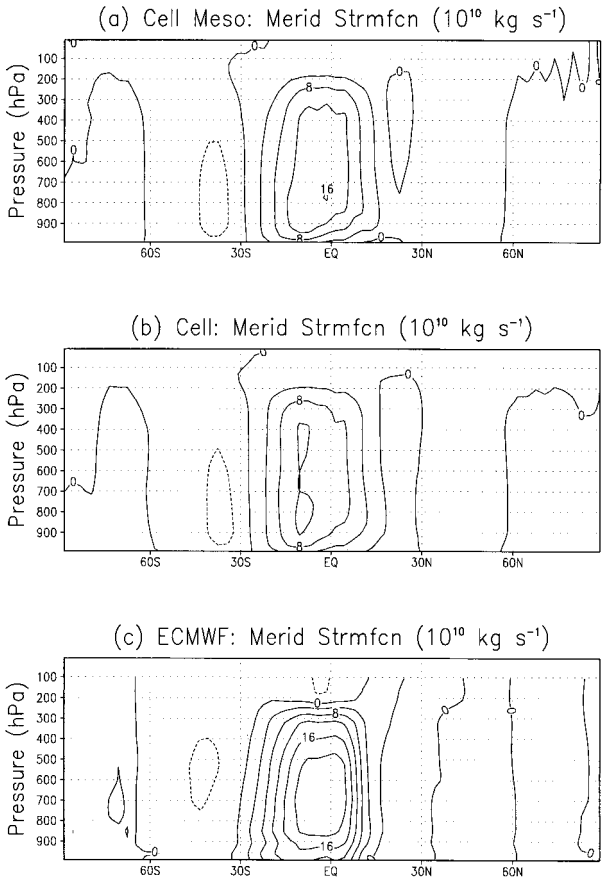

FIG. 9. Meridional streamfunctions for (a) Cell Meso, (b) Cell, and (c) ECMWF.

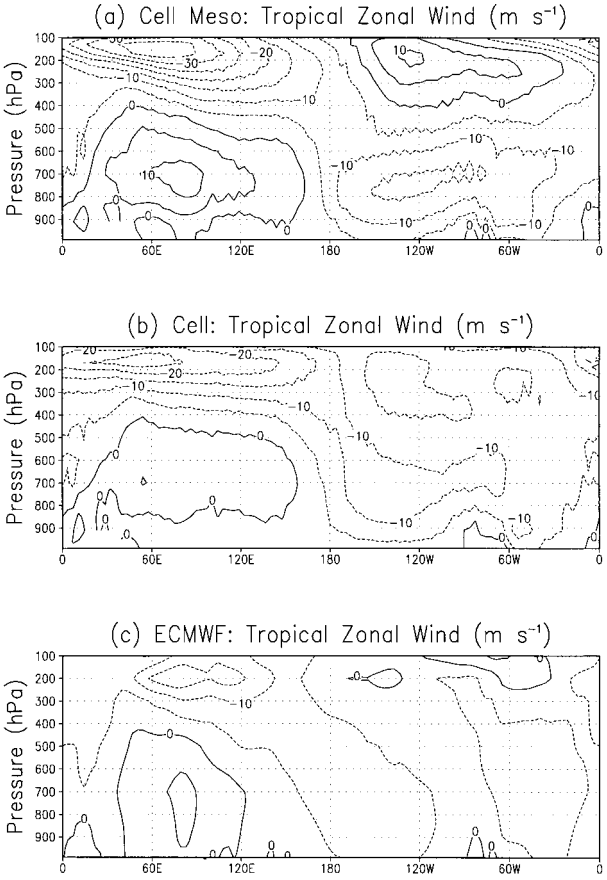

FIG. 10. Zonal wind averaged from 5°N to 5°S for (a) Cell Meso, (b) Cell, and (c) ECMWF.

tropical troposphere is also evident in the distribution of precipitable water (Fig. 7). Although still somewhat drier in the Tropics than the National Acronautics and Space Administration's (NASA) Water Vapor Project (NVAP) observations, the moister Cell Meso precipitable-water field matches NVAP more closely. Differences in precipitable water between Cell Meso and Cell are *t*-test significant at 0.995 for most tropical and midlatitude regions with appreciable precipitable water.

As noted earlier, the cumulus-parameterization moisture source (Fig. 2) extends to higher altitudes in the tropical troposphere when mesoscale processes are treated. The effect on water-vapor mixing ratios in the upper troposphere and lower stratosphere is illustrated in Fig. 8. The mesoscale circulations generally increase mixing ratios, confining their negative bias relative to Stratospheric Aerosol and Gas Experiment (SAGE) observations to below 220 hPa. The positive bias in the north polar region is much more pronounced in Cell Meso. Since mixing ratios throughout the Tropics are closer to SAGE observations below 100 hPa and the convective moisture source is smaller toward the Poles, this bias is probably more strongly related to meridional transport of water vapor in SKYHI than convection. Radiative cooling associated with this bias also is apparent in the colder temperatures near the Poles in Cell Meso in Fig. 6a. (Most of the changes between Cell Meso and Cell are *t*-test significant at the 0.995 level.)

The mesoscale circulations produce a fairly complex pattern of changes in the precipitation field (not shown) with little evidence of large, coherent differences between Cell Meso and Cell.

The differences in the structure of the cumulus-parameterization heat source result in different structures in the total diabatic heating field. The latter differences, in turn, lead to differences in the dynamics of the general circulation. Two broad measures of this impact can be seen in the Hadley and Walker circulations. Figure 9 shows that the mean meridional (Hadley) circulation is strengthened by the mesoscale circulations. The differences between Cell Meso and Cell are *t*-test significant at 0.95 between the Tropics and about 10°S. (The mean meridional circulation is defined as $2\pi a_e \cos\phi g^{-1} \int_p^{p_g} [v]\, dp'$, where ϕ, a_e, $[v]$, and p_g denote latitude, the earth's radius, time-mean zonally averaged meridional velocity, and pressure at earth's surface, respectively.)

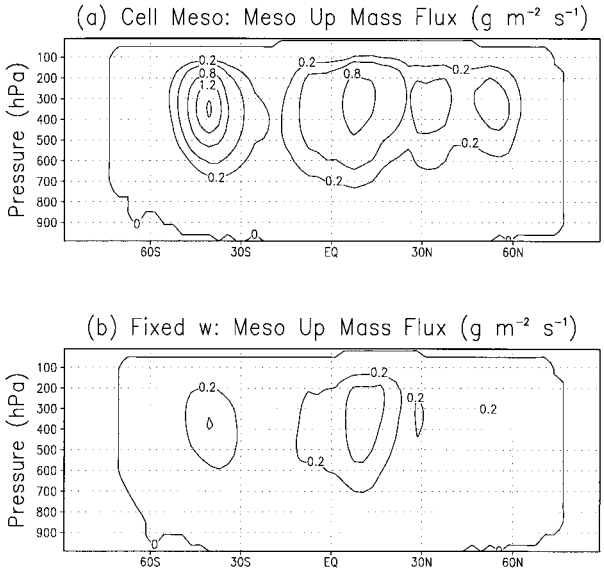

FIG. 11. Mass fluxes in mesoscale updrafts for (a) Cell Meso and (b) Fixed *w*. Contour levels: 0, 0.2, 0.4, 0.8, 1.2, 1.5 g m^{-2} s^{-1}.

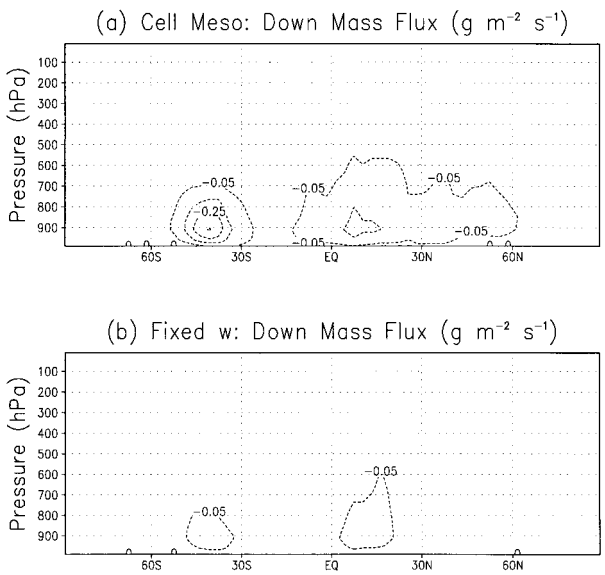

FIG. 12. Mass fluxes in mesoscale and convective-cell downdrafts for (a) Cell Meso and (b) Fixed *w*.

Midtroposphere meridional heating gradients are stronger near the equator in Cell Meso than Cell (Figs. 1a,b). Stronger equatorward diabatic-heating gradients increase the intensity of the Hadley circulation (Holton 1992, chapter 10). Even in Cell Meso, the Hadley circulation remains weaker than in the European Centre for Medium-Range Weather Forecasts (ECMWF) analysis, possibly due to an absence of horizontal-momentum transport in the cumulus parameterization. [Helfand (1979) and Gregory et al. (1997) find that convective momentum transport has important effects on the momentum balance, although their conclusions as to its effect on the strength of the Hadley circulation differ.]

Hartmann et al. (1984) find that changes in the vertical structure of heating associated with mesoscale circulations in tropical cloud clusters change the Walker circulation in a linear steady-state model. Figure 10 shows that these mesoscale circulations alter the structure of the Walker circulation in SKYHI also. Figure 10 shows the zonal wind averaged over a tropical band of latitudes from 5°N to 5°S. The Walker circulation, characterized by strong westerly inflow at low levels west of 135°E, is clearly stronger when mesoscale processes are present. The ECMWF analysis exhibits low-level Walker westerly inflow whose magnitude is between the Cell Meso and Cell integrations. When mesoscale processes are included, the low-level Walker westerlies extend closer to the surface than in Cell. Westerlies extend to the surface over about 60° in the ECMWF analysis. Upper-level Walker easterlies are stronger than in the ECMWF analysis in both Cell Meso and Cell. Elsewhere in the tropical circulation, the ECMWF analysis shows a band of westerlies in the upper troposphere over South America. These do not exist in the Cell integration but develop (even more strongly than analyzed) when mesoscale circulations exist. (The differences between Cell Meso and Cell for the low-level Walker westerlies are *t*-test significant at 0.995. The westerly differences over South America and the upper-level Walker easterly differences are generally significant at 0.95.)

6. Impact of parameterizing convective vertical velocity

A central aspect of Donner's (1993) cumulus parameterization is its inclusion of convective vertical velocities. The purpose of including them is to ensure a physical basis for driving convective microphysics, which are in turn a major source of condensate for mesoscale circulations. The convective vertical velocities are calculated using a steady-state equation for convective vertical momentum, in which vertical advection of vertical momentum is balanced by buoyancy, condensate loading, and entrainment. This section considers the role of spatial and temporal variations in convective vertical velocity, primarily by comparing Cell Meso with Fixed *w*, in which the procedure described in section 3 is used to fix vertical velocities for each ensemble member. Note that Fixed *w* still allows for a major source of nonlinearity between convective vertical velocity and microphysics, since there are appreciable variations in convective vertical velocity among ensemble members.

The general effect of parameterizing spatial and temporal variations in convective vertical velocity is to intensify the mesoscale circulations associated with deep convection. This effect can be seen very clearly in smaller mass fluxes in both the mesoscale updrafts (Fig. 11) and downdrafts (Fig. 12). It is also somewhat evident

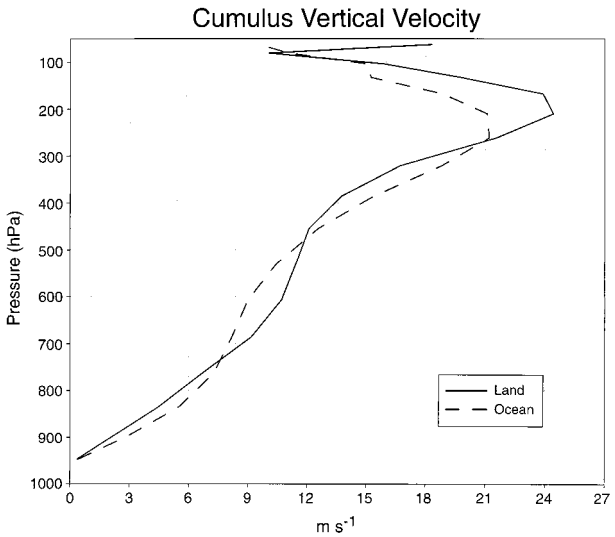

FIG. 13. Cumulus vertical velocities averaged separately over all land and oceanic points during convective events.

in the total convective-system mass fluxes shown in Fig. 5, where the vertical structure of the mass fluxes in Fixed *w* resembles more closely those of Cell Meso, but the magnitudes are greater and approach those of Cell.

Understanding the reasons for enhanced mesoscale activity when convective vertical velocity is parameterized requires further study. Several factors are relevant. The parameterized convective vertical velocities need not produce average convective vertical velocities identical to those imposed in Fixed *w*. Further, the intensity of mesoscale activity in Donner's (1993) parameterization generally increases with convective vertical velocity. This behavior is a result of decreased parcel transit times in convective cells as vertical velocity increases. Decreased transit times diminish the extent to which microphysical processes such as collection and collision can operate, reducing the cell precipitation and increasing the condensate available for building mesoscale stratiform clouds. Since transit times are nonlinear (inversely proportional) to convective vertical velocities, mesoscale intensities would differ in a Fixed *w* integration, even if average convective vertical velocities were identical to imposed velocities.

7. Observational evidence regarding the subgrid character of convective systems

The foregoing sections have illustrated that the mesoscale circulations associated with deep convection play important roles in determining convective-system mass fluxes and impact the thermodynamic and dynamic character of the general circulation. The intensity of these mesoscale circulations is related to spatial and temporal variations in convective vertical velocity. Convective systems with associated mesoscale cloud sys-

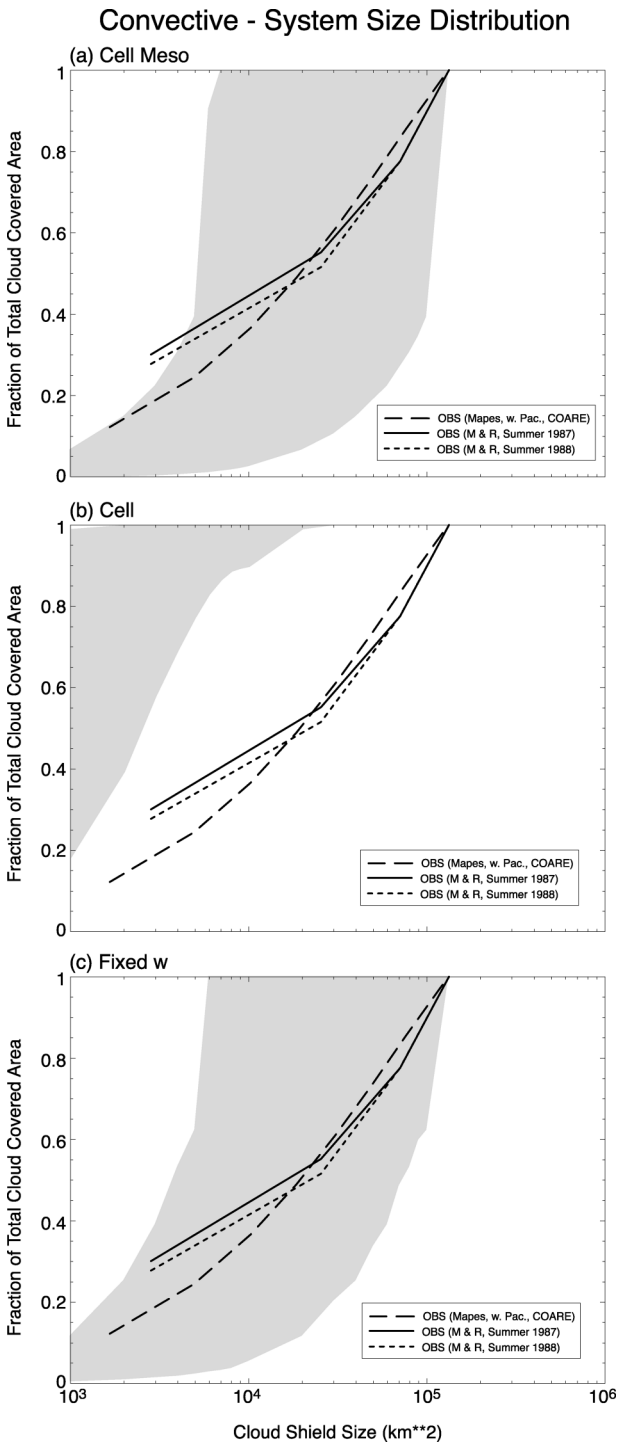

FIG. 14. Convective-system size distributions for (a) Cell Meso, (b) Cell, and (c) Fixed *w*. The shaded band indicates the size distributions for SKYHI assuming from 1 to 20 convective systems per grid box.

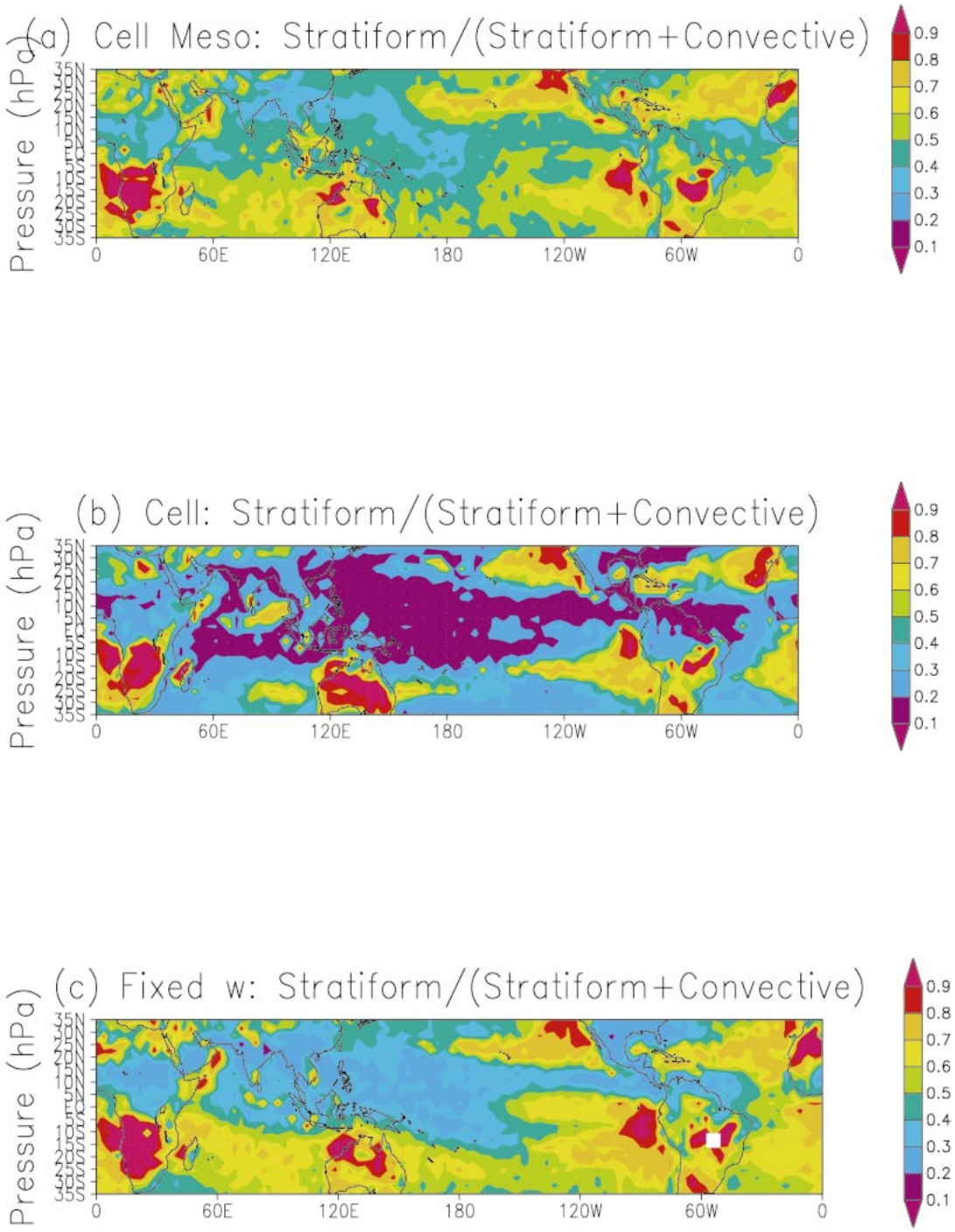

FIG. 15. Ratios of stratiform to the sum of stratiform and convective precipitation for (a) Cell Meso, (b) Cell, (c) Fixed *w*, and (d) TRMM.

tems are very complex and are of necessity represented in an idealized manner in parameterizations such as that used here. This section will consider observational evidence that relates directly to some of the most important subgrid aspects of the parameterization, namely, those regarding the importance of mesoscale and convective components of the systems and the spatial and temporal variations in convective vertical velocities.

Spatial and temporal variations in convective vertical velocity, as represented in Donner's (1993) parameter-

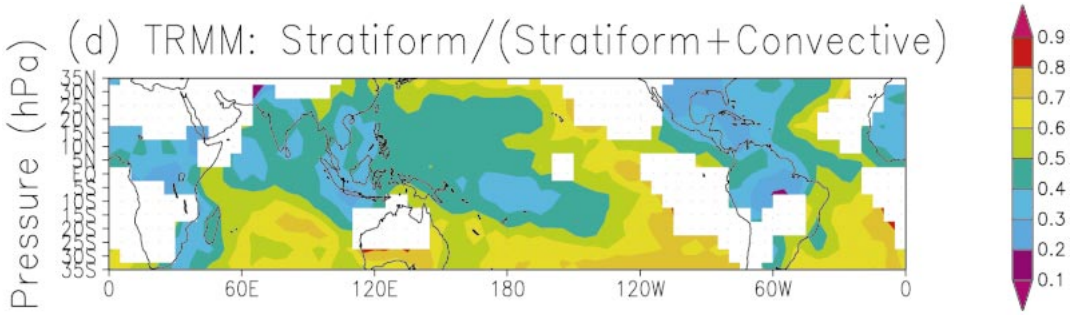

FIG. 15. (*Continued*)

ization, depend on the variations in large-scale vertical profiles of temperature and moisture. These variations go beyond variations in quantities such as CAPE. For example, observations have shown that land convective vertical velocities generally exceed those of oceanic convection between 500 and 800 hPa, even for similar CAPE (Lucas et al., 1994, Fig. 3). This behavior is also evident in Fig. 13, which shows the composite vertical velocities for convective ensembles over land and ocean for CAPE values between 1500 and 3000 J kg^{-1}. Note that these are conditional averages including only cases when convection is present. The frequency of such cases decreases with height; only the most penetrative ensemble members reach the upper troposphere, and, of these, only the most intense reach the greatest altitudes. The vertical velocities in Fig. 13 include all land and oceanic points in SKYHI whose CAPE is within the indicated range, so a direct comparison with the oceanic and land convective vertical velocities in Lucas et al. (1994) is not possible. The convective vertical velocities of Lucas et al. (1994), which generally show larger differences between oceanic and land convection than SKYHI, are drawn from several field experiments. The differences in SKYHI oceanic and land vertical velocities are the result of different shapes in the temperature profiles over land and ocean. The CAPE values for the composite thermodynamic soundings over ocean and land are 2002 and 2006 J kg^{-1}, respectively. For the most penetrative ensemble, the oceanic cumulus cells have a depth of 750 hPa, but the maximum virtual temperature difference between the cells and the large-scale environment when the parameterization is applied to this composite is 4.0 K. For land, the corresponding values are 660 hPa and 5.9 K. This result is consistent with the assessment of Lucas et al. (1994), who associated weaker oceanic convection with ''skinny'' positive areas on thermodynamic soundings, compared to ''fat'' areas for land. (Note that lower land convective vertical velocities at pressures less than 500 hPa are also consistent with this explanation based on the different shapes of thermodynamic profiles over land and ocean.)

Variations in convective vertical velocities for similar values of CAPE are among the more subtle of vertical-velocity variations. In light of the results presented in section 6 showing the importance of spatial and temporal variations in convective vertical velocities, it is encouraging that the idealized representation of cumulus dynamics in Donner (1993) can capture some aspects of these variations.

The relative magnitude of convective and stratiform precipitation is an important characteristic of convective systems. Satellite-based studies of the sizes of convective systems provide a constraint, since convective cells generally occupy a much smaller area than stratiform shields. Figure 14 shows satellite-based size distributions of convective shields for the oceanic warm pool (Mapes and Houze 1993) and for the Tropics (Machado and Rossow 1993). The shaded area on Fig. 14 indicates the corresponding range for convective-system areas in SKYHI, assuming 1–20 convective systems per grid box. [Donner's (1993) parameterization provides the total areas of convective systems but not sizes of individual systems.] Satellite-based observations that lie below or to the right of the SKYHI bands are inconsistent with the model results, since even the largest possible systems in SKYHI would be smaller than observed. The results in Fig. 14 show that the Cell integration is not capable of matching observed system sizes. The mesoscale circulations are clearly necessary for the SKYHI results to be consistent with observations. Spatial and temporal variations shift the sizes of convective systems toward smaller sizes, as can be seen by comparing the SKYHI bands for Cell Meso and Fixed *w*, but the absence of these variations does not render the convective-system sizes inconsistent with observations.

Another means of assessing the relative roles of convective and stratiform processes in convective systems is to examine the ratios of stratiform to convective precipitation as measured by the Tropical Rainfall Measuring Mission (TRMM; available online at http://lake.nascom.nasa.gov/data/dataset/TRMM). TRMM convective and stratiform rain amounts have been compared with Kwajalein ground-based radar by Schumacher and Houze (2000) and found to be in reasonable agreement, within 10% for both convective and stratiform rain. Figure 15 illustrates the ratios of stratiform

to convective precipitation. For comparison with TRMM, all SKYHI stratiform and convective precipitation is included in this comparison. The Cell Meso and TRMM patterns show many areas of agreement. The Fixed *w* integration, however, has smaller stratiform ratios in many areas (west Pacific, tropical east Pacific, equatorial Africa, Arabian Sea, Bay of Bengal) than Cell Meso. The stratiform ratio over much of the west Pacific is only 20%–30% in Fixed *w,* compared to 30%–50% in Cell Meso and 40%–50% in TRMM. Spatial and temporal variations in convective vertical velocity are important in improving agreement of the partitioning of stratiform and convective precipitation between SKYHI and observations. In extreme contrast, in Cell, the SKYHI field shows vastly lower stratiform precipitation ratios in regions of deep convection than TRMM.

There are large regional variations in the ratios of stratiform to convective precipitation in Fig. 15. No single controlling parameter is evident for the stratiform precipitation ratio. Deeper clouds, often associated with larger values of CAPE, generally have less condensate available for mesoscale circulations than shallower clouds; the longer transit distance for parcels moving through such clouds enables convective microphysics to remove more condensate as precipitation. For clouds of comparable depth, higher vertical velocities imply shorter parcel transit times, and these clouds have more condensate available to build mesoscale circulations. The patterns in Fig. 15 are aggregates of these and other competing processes. The local minima in the stratiform ratio in Fig. 15 over equatorial Africa, the western and central Pacific, and extreme eastern equatorial Atlantic are all near areas of CAPE maxima. The effect of convective vertical velocity on the stratiform ratio is evident for the land and oceanic composite profiles (Fig. 13). The fraction of condensate not precipitated from convective cells is higher for all but the shallowest ensemble member for the land convection with its higher vertical velocities, as much as 30% higher for an ensemble member detraining in the midtroposphere and 12% higher for the deepest ensemble member, even though it is 90 hPa deeper than for the oceanic profile. The rough agreement between the stratiform ratios for TRMM and Cell Meso suggests that some of these competing physical mechanisms are captured in the parameterization.

8. Conclusions

By adding cumulus-scale vertical velocities to mass fluxes in a parameterization for deep convection, a physically consistent treatment of cumulus-scale microphysics has been developed. Explicit parameterizations for the mesoscale components of deep convection can be constructed using the vapor and condensate detrainment from deep convective cells parameterized in this way. Implementation of a parameterization including microphysics and mesoscale components in a GCM shows that global contributions from the mesoscale components are important relative to those from the deep convective towers.

Heat and moisture sources and sinks differ somewhat when mesoscale processes are parameterized, but mass fluxes are very different. Substantially more detrainment occurs in the midtroposphere, and mass fluxes are reduced, when mesoscale processes are parameterized. Implications for tracer transport by deep convection are likely to be important.

Mesoscale circulations associated with deep convection influence the atmospheric general circulation in several ways. Convective-system moistening extends to greater heights in the upper troposphere, reducing a dry bias relative to SAGE observations there but producing a moist bias in the lower stratosphere. The tropical troposphere is generally more humid, and the Walker and Hadley circulations are both intensified by these mesoscale circulations.

Mesoscale circulations are more intense when convective vertical velocities are parameterized than when typical velocities are imposed. Nonlinearities between convective vertical velocities and microphysics play a role in this behavior.

Several mesoscale and related subgrid aspects of the parameterization are consistent with field and observational studies. Convective vertical velocities are greater over land than ocean, even for similar CAPE values. The size distribution of convective systems is consistent with satellite observations only if mesoscale processes are parameterized. Ratios of stratiform to convective precipitation have a pattern generally similar to TRMM observations, and their magnitudes match TRMM more closely if convective vertical velocities are parameterized.

Acknowledgments. Brian Soden assisted in obtaining the NVAP and SAGE observations. Cathy Raphael and Jeff Varanyak assisted in drafting the figures. Laura Fowler (Colorado State University) was helpful in identifying TRMM data sources. We thank Matthias Steiner (Princeton University) and Courtney Schumacher (University of Washington) for their insights regarding TRMM convective and stratiform rainfall partitioning. Brian Mapes provided satellite size distributions for convective systems for the oceanic warm pool. Comments on the initial version of the manuscript by Martin Köhler and Joe Sirutis are much appreciated. Two thorough anonymous reviews of the initial version of the manuscript raised several of the observational issues addressed in this paper and yielded a clearer presentation of the material.

APPENDIX A

Symbols and Units

Symbol	Description	Units
a_e	Earth's radius	m
a_1	Fractional area of an arbitrary ensemble member	dimensionless
CAPE	Convective available potential energy	J kg^{-1}
c_p	Specific heat at constant pressure	J kg^{-1} K^{-1}
g	Gravity constant	m s^{-2}
I_1	Closure integral	J kg^{-1} s^{-1}
I_2	Convective-onset integral	Pa
L_1	Latent heat of vaporization	J kg^{-1}
L_2	$-L_1$	J kg^{-1}
L_3	Latent heat of sublimation	J kg^{-1}
L_4	$-L_3$	J kg^{-1}
L_5	Latent heat of fusion	J kg^{-1}
L_6	$-L_5$	J kg^{-1}
p	Pressure	Pa
p_g	Pressure at earth's surface	Pa
p_0	Reference pressure	Pa
p_1	Pressure at first GCM level above ground	Pa
q	Vapor mixing ratio	kg(water) kg^{-1}
q_c	Condensate mixing ratio	kg(water) kg^{-1}
q_T	Total-water mixing ratio	kg(water) kg^{-1}
Q_R	Convective-system moisture source	kg(water) kg^{-1} s^{-1}
Q_T	Convective-system thermal source	K s^{-1}
R_d	Gas constant for dry air	J kg^{-1} K^{-1}
T	Temperature	K
T_ρ	Density temperature	K
$T_{\rho p}$	Density temperature of lifted parcel	K
t	Time	s
t_0	Start time for convective-onset integral	s
ϵ	Ratio of molecular weights, water to dry air	dimensionless
υ	Meridional velocity	m s^{-1}
π	Ratio of potential temperature to temperature	dimensionless
θ	Potential temperature	K
ω	Vertical (pressure) velocity	Pa s^{-1}
γ_1	Condensation rate	kg(water) kg^{-1} s^{-1}
γ_2	Evaporation rate	kg(water) kg^{-1} s^{-1}
γ_3	Deposition rate	kg(water) kg^{-1} s^{-1}
γ_4	Sublimation rate	kg(water) kg^{-1} s^{-1}
γ_5	Freezing rate	kg(water) kg^{-1} s^{-1}
γ_6	Melting rate	kg(water) kg^{-1} s^{-1}
ϕ	Latitude	
τ_m	Mesoscale lifetime	s

The following apply generally:

$(\,)_b$	refers to the base of a cell updraft.
$(\,)_g$	refers to the surface pressure.
$(\,)_{\mathrm{LFC}}$	refers to the level of free convection.
$(\,)_{\mathrm{LZB}}$	refers to the level of zero buoyancy.
$(\,)'$	refers to a departure from a large-scale average.
$(\,)^*$	refers to a property or process within a convective system.
$\overline{(\,)}$	refers to a large-scale average.
$[\,]$	refers to a zonal average.
$\widetilde{(\,)}$	refers to normalization by a_1.

APPENDIX B

Implementation Details

a. Closure integral

The closure integral I_1 is obtained taking the local time derivative of CAPE:

$$\text{CAPE} = \int_{p_{\text{LZB}}}^{p_{\text{LFC}}} R_d(T_{\rho p} - \overline{T}_\rho)\, d\ln p. \tag{B1}$$

The density temperature T_ρ is defined as

$$T_\rho = T\frac{1 + q/\epsilon}{1 + q_T}, \tag{B2}$$

where ϵ is the ratio of molecular weights of water to dry air and q_T is the total water mixing ratio. The density temperature of a parcel lifted without dilution from the GCM level nearest the ground is denoted as $T_{\rho p}$. In the present application, prognostic cloud condensate is not used, so the density temperature does not include condensate effects. The closure integral I_1 is simplified in the following, as a result.

The components of the derivative related to convection then are equated to $a_1(p_b)I_1$, yielding

$$\frac{I_1}{R_d} = \int_{p_{\text{LZB}}}^{p_g} \left\langle -\frac{\tilde{Q}_T(\epsilon + \overline{q})}{\epsilon(1 + \overline{q})} - \frac{\overline{T}(1 - \epsilon)\tilde{Q}_R}{\epsilon(1 + \overline{q})^2} + \frac{\partial T_{\rho p}}{\partial \overline{T}_\rho(p_1)}\left\{\frac{\tilde{Q}_T(p_1)[\epsilon + \overline{q}(p_1)]}{\epsilon[1 + \overline{q}(p_1)]} + \frac{\overline{T}(p_1)(1 - \epsilon)\tilde{Q}_R(p_1)}{\epsilon[1 + \overline{q}(p_1)]^2}\right\}\right\rangle d\ln p. \tag{B3}$$

Note that (B3) also includes a contribution between p_g and p_{LFC} (convective inhibition) not in (B1), but this simplification should have little effect.

b. Other details

As noted in section 2, ice clouds are generally treated as in Donner et al. (1997). A small-particle correction for large-scale ice clouds, described in section 2.4 of Donner et al. (1997), was not actually applied there but is applied in the present study. Radiative properties of convective anvils are also treated as in Donner et al. (1997), except that the convective precipitation rate required by Slingo (1987) is obtained directly from the convective-system parameterization instead of SAA.

In GCM application, flows occasionally develop that do not fall within the patterns for which the parameterization was designed. These situations are handled as described subsequently. These situations are uncommon but are summarized here for completeness.

If the least penetrative ensemble is not at least 500 hPa deep, the mesoscale component of the convective system does not form. Instead, the convective system in these cases consists only of convective cells (cf. section 2a, Donner 1993).

Deposition in mesoscale anvils follows the procedure described in section 2b(3) of Donner (1993), except when an inversion exists at a level within the mesoscale circulation, in which case no additional in situ deposition occurs with mesoscale ascent unless the inversion top is reached. Also, note that a term $\overline{q}(p)/\tau_m$, where τ_m is the mesoscale lifetime, should be added to the left side of the first expression in Donner's (1993) section 2b(3).

If the base of the mesoscale updraft is within 200 hPa of the ground, no mesoscale downdraft forms. Consistent with the highly simplified treatment of mesoscale downdrafts in Donner (1993), this represents cases where insufficient evaporative cooling to drive a mesoscale downdraft occurs.

The base of the mesoscale updraft is at the level closest to the ground where the ensemble as a whole begins to provide water vapor to its environment, rather than where the least penetrative member does so. The latter approach is taken in Donner (1993). Also, should an ensemble fail to detrain water vapor, only condensate is transferred to the anvil, whose base is taken to be the level where the least penetrative member's vertical velocity vanishes.

REFERENCES

Alexander, D. G., and W. R. Cotton, 1998: The use of cloud-resolving simulations of mesoscale convective systems to build a mesoscale parameterization scheme. *J. Atmos. Sci.*, **55,** 2137–2161.

Allen, D. J., K. E. Pickering, and A. Molod, 1997: An evaluation of deep convective mixing in the Goddard Chemical Transport Model using International Satellite Cloud Climatology Project cloud parameters. *J. Geophys. Res.,* **102,** 25 467–25 476.

Arakawa, A., and W. H. Schubert, 1974: Interaction of a cumulus cloud ensemble with the large-scale environment: Part 1. *J. Atmos. Sci.,* **31,** 674–701.

Boucher, O., H. Le Treut, and M. B. Baker, 1995: Precipitation and radiation modelling in a GCM: Introduction of cloud microphysical processes. *J. Geophys. Res.*, **100,** 16 395–16 414.

DelGenio, A. D., M.-S. Yao, W. Kovari, and K.-W. Lo, 1996: A prognostic cloud water parameterization for global climate models. *J. Climate*, **9,** 270–304.

Donner, L. J., 1993: A cumulus parameterization including mass fluxes, vertical momentum dynamics, and mesoscale effects. *J. Atmos. Sci.*, **50,** 889–906.

——, C. J. Seman, B. J. Soden, R. S. Hemler, J. C. Warren, J. Ström, and K.-N. Liou, 1997: Large-scale ice clouds in the GFDL SKYHI general circulation model. *J. Geophys. Res.,* **102,** 21 745–21 768.

Fowler, L. D., D. A. Randall, and S. A. Rutledge, 1996: Liquid and ice cloud microphysics in the CSU General Circulation Model. Part I: Model description and simulated microphysical processes. *J. Climate,* **9,** 489–529.

Garratt, J. R., 1994: *The Atmospheric Boundary Layer*. Cambridge University Press, 316 pp.

Gregory, D., and P. R. Rowntree, 1990: A mass flux convection scheme with representation of cloud ensemble characteristics and stability-dependent closure. *Mon. Wea. Rev.,* **118,** 1483–1506.

——, R. Kershaw, and P. M. Inness, 1997: Parametrization of momentum transport by convection. II. Tests in single-column and general circulation models. *Quart. J. Roy. Meteor. Soc.,* **123,** 1153–1183.

Hack, J. J., 1994: Parameterization of moist convection in the National Center for Atmospheric Research community climate model (CCM2). *J. Geophys. Res.,* **99,** 5551–5568.

Hall, A., and S. Manabe, 1999: The role of water vapor feedback in unperturbed climate variability and global warming. *J. Climate,* **12,** 2327–2346.

Hamilton, K., R. J. Wilson, J. D. Mahlman, and L. J. Umscheid, 1995: Climatology of the SKYHI Troposphere-Stratosphere-Mesosphere General Circulation Model. *J. Atmos. Sci.,* **52,** 5–43.

Harrison, E. F., P. Minnis, B. R. Barkstrom, V. Ramanathan, R. D. Cess, and G. G. Gibson, 1990: Seasonal variation of cloud radiative forcing derived from the Earth Radiation Budget Experiment. *J. Geophys. Res.,* **95,** 18 687–18 703.

Hartmann, D. L., H. H. Hendon, and R. A. Houze, 1984: Some implications of the mesoscale circulations in tropical cloud clusters for large-scale dynamics and climate. *J. Atmos. Sci.,* **41,** 113–121.

Helfand, H. M., 1979: The effect of cumulus friction on the simulation of the January Hadley circulation by the GLAS model of the general circulation. *J. Atmos. Sci.,* **36,** 1827–1843.

Holton, J. R., 1992: *An Introduction to Dynamic Meteorology*. Academic Press, 511 pp.

Houze, R. A., 1989: Observed structure of mesoscale convective systems and implications for large-scale heating. *Quart. J. Roy. Meteor. Soc.,* **115,** 425–461.

Igau, R. C., M. A. LeMone, and D. Wei, 1999: Updraft and downdraft cores in TOGA COARE: Why so many buoyant downdraft cores? *J. Atmos. Sci.,* **56,** 2232–2245.

Kuo, H.-L., 1974: Further studies of the parameterization of the influence of cumulus convection on large-scale flow. *J. Atmos. Sci.,* **31,** 1232–1240.

Leary, C. A., and R. A. Houze Jr., 1980: The contribution of mesoscale motions to the mass and heat fluxes of an intense tropical convective system. *J. Atmos. Sci.,* **37,** 784–796.

LeMone, M. A., and E. J. Zipser, 1980: Cumulonimbus vertical velocity events in GATE. Part I: Diameter, intensity, and mass flux. *J. Atmos. Sci.,* **37,** 2444–2457.

Le Treut, H., Z.-X. Li, and M. Forichan, 1994: Sensitivity of the LMD general circulation model to greenhouse forcing associated with two different cloud water parameterizations. *J. Climate,* **7,** 1827–1841.

Lin, C., and A. Arakawa, 1997: The macroscopic entrainment processes of simulated cumulus ensemble. Part I: Entrainment sources. *J. Atmos. Sci.,* **54,** 1027–1043.

Lucas, C., E. J. Zipser, and M. A. LeMone, 1994: Vertical velocity in oceanic convection off tropical Australia. *J. Atmos. Sci.,* **51,** 3183–3193.

Machado, L. A. T., and W. B. Rossow, 1993: Structural characteristics and radiative properties of tropical cloud clusters. *Mon. Wea. Rev.,* **121,** 3234–3260.

Mapes, B. E., and R. A. Houze Jr., 1993: Cloud clusters and superclusters over the oceanic warm pool. *Mon. Wea. Rev.,* **121,** 1398–1415.

Ose, T., 1993: An examination of the effects of explicit cloud water in the UCLA GCM. *J. Meteor. Soc. Japan,* **71,** 93–109.

Rasch, P. J., and J. E. Kristjánsson, 1998: A comparison of the CCM3 model climate using diagnosed and predicted condensate parameterizations. *J. Climate,* **11,** 1587–1614.

Raymond, D. J., and A. M. Blythe, 1986: A stochastic model for nonprecipitating cumulus clouds. *J. Atmos. Sci.,* **43,** 2708–2718.

Ricard, J. L., and J. F. Royer, 1993: A statistical cloud scheme for use in an AGCM. *Ann. Geophys.,* **11,** 1095–1115.

Rotstayn, L. D., 1997: A physically based scheme for the treatment of stratiform clouds and precipitation in large-scale models. Part I: Description and evaluation of the microphysical processes. *Quart. J. Roy. Meteor. Soc.,* **123,** 1227–1282.

Schumacher, C., and R. A. Houze Jr., 2000: Comparison of radar data from the TRMM satellite and Kwajalein oceanic validation site. *J. Appl. Meteor.,* **39,** 2151–2164.

Slingo, J. M., 1987: The development and verification of a cloud prediction scheme for the ECMWF model. *Quart. J. Roy. Meteor. Soc.,* **113,** 899–927.

Smith, R. N. B., 1990: A scheme for predicting layer clouds and their water content in a general circulation model. *Quart. J. Roy. Meteor. Soc.,* **116,** 435–460.

Thompson, R. M., S. W. Payne, E. E. Recker, and R. J. Reed, 1979: Structure and properties of synoptic-scale wave disturbances in the intertropical convergence zone of the eastern Atlantic. *J. Atmos. Sci.,* **36,** 53–72.

Tiedtke, M., 1989: A comprehensive mass flux scheme for cumulus parameterization in large-scale models. *Mon. Wea. Rev.,* **117,** 1779–1800.

——, 1993: Representation of clouds in large-scale models. *Mon. Wea. Rev.,* **121,** 3030–3061.

Wetherald, R. T., 1996: *Feedback processes in the GFDL R30-14 Level General Circulation Model.* NATO ASI Series, Vol. I, No. 34, Springer-Verlag 331 pp.

Zhang, G., and N. A. McFarlane, 1995: Sensitivity of climate simulations to the parameterization of cumulus convection in the Canadian Climate Centre General Circulation Model. *Atmos.–Ocean,* **33,** 407–446.

——, J. T. Kiehl, and P. J. Rasch, 1998: Response of climate simulation to a new convective parameterization in the National Center for Atmospheric Research Community Climate Model (CCM3). *J. Climate,* **11,** 2097–2115.